

1 Reclaiming Hand Functions after Complete Spinal Cord Injury with 2 Epidural Brain-Computer Interface

3
4 Dingkun Liu, Ph.D.^{1#}, Yongzhi Shan, M.D., Ph.D.^{2#}, Penghu Wei, M.D., Ph.D.^{2#}, Wenzheng Li,
5 M.S.¹, Honglai Xu, Ph.D.³, Fangshuo Liang, B.S.¹, Tao Liu, M.S.³, Guoguang Zhao, M.D., Ph.D.^{2*},
6 Bo Hong, Ph.D.^{1*}

7
8 ¹Department of Biomedical Engineering, School of Medicine, Tsinghua University, Beijing, China.

9 ²Department of Neurosurgery, Xuanwu Hospital of Capital Medical University, National Medical
10 Center for Neurological Diseases, Beijing, China.

11 ³Neuracle Technology Co., Shanghai, China.

12

13 [#] Equal contribution

14 ^{*} Corresponding author

15

16 E-mail: hongbo@tsinghua.edu.cn

17

18

19

20 **Abstract:**

21 **Background:**

22 Spinal cord injuries significantly impair patients' ability to perform daily activities independently.
23 While cortically implanted brain-computer interfaces (BCIs) offer high communication bandwidth
24 to assist and rehabilitate these patients, their invasiveness and long-term stability limits broader
25 adoption.

26 **Methods:**

27 We developed a minimally invasive BCI with 8 chronic epidural electrodes above primary
28 sensorimotor cortex to restore hand functions of tetraplegia patients. With wireless powering and
29 neural data transmission, this system enables real-time BCI control of hand movements and hand
30 function rehabilitation in home use. A complete spinal cord injury (SCI) patient with paralyzed hand
31 functions was recruited in this study.

32 **Results:**

33 Over a 9-month period of home use, the patient achieved an average grasping detection F1-score of
34 0.91, and a 100% success rate in object transfer tests, with this minimally invasive BCI and a
35 wearable exoskeleton hand. This system allowed the patient to perform eating, drinking and other
36 daily tasks involving hand functions. Additionally, the patient showed substantial neurological
37 recovery through consecutive BCI training, regaining the ability to hold objects without BCI. The
38 patient exhibited a 5-point improvement in upper limb motor scores and a 27-point increase in the
39 action research arm test (ARAT). A maximal increase of 12.2 μ V was observed in the peak of

40 NOTE: This preprint reports new research that has not been certified by peer review and should not be used to guide clinical practice.

41 connections.

42 **Conclusions:**

43 In a tetraplegia patient with complete spinal cord injury, an epidural minimally invasive BCI
44 assisted the patient's hand grasping to perform daily tasks, and 9-month consecutive BCI use
45 significantly improved the hand functions.

46

47 Introduction

48 Spinal cord injuries (SCI) can lead to permanent paralysis of the limbs, especially when the injury
49 occurs in the cervical region, resulting in the loss of motor function in all four limbs. Implantable
50 brain-computer interfaces (BCIs) present a novel solution to help patients regain partial motor
51 functions^{1,2}. Combined with epidural spinal cord stimulation, these interfaces can facilitate
52 functional rehabilitation^{3,4}. Current research on implantable BCIs primarily focuses on increasing
53 their communication bandwidth for better motor control⁵. However, the long-term efficacy and
54 reliability of these systems are often hindered by safety issues^{6,7}, which poses an challenge to
55 reduce the invasiveness' of implantable BCIs to achieve an balance between performance and
56 safety. From the perspective of motor function rehabilitation, BCIs combined with epidural spinal
57 cord stimulation have been shown to enhance axonal excitability, induce closed-loop electrical
58 activity, and promote active rehabilitation of the brain-spinal cord pathways^{3,8}. This combination
59 can potentially restore voluntary walking abilities in patients^{3,8}. However, it remains unclear
60 whether the brain-spinal cord neural connections can also be repaired through BCI-induced
61 intrinsic neural coupling without external electrical stimulation.

62 In our previous study, using epidural electrodes and wireless communication, an implantable BCI
63 system was developed and validated in animal models. The system ensures long-term safety and
64 effectiveness through its battery-free, bidirectional design and epidural electrodes that keep the
65 brain tissue intact. In this study, we utilized the NEO BCI system to develop a long-term hand
66 movement assistance system for a patient with complete C4 spinal cord injury resulting in
67 tetraplegia. We investigated whether neural rehabilitation could be achieved through the coupling
68 of cortical descending control signals and ascending sensory signals at the injury site, without
69 relying on external electrical stimulation.

70 Methods

71 The Epidural Minimally Invasive BCI

72 The minimally invasive BCI, named NEO (Neural Electronics Opportunity), has an implant and
73 an external processor that are linked with transcutaneous wireless communication. The
74 exoskeleton hand (pneumatic glove wore on the patient's right hand, Fubo Co.) is driven by the
75 BCI external processor wirelessly as well (Fig. 1a). NEO includes two sets of coils: the first set
76 supplies power for the implant through near-field induction, and the second transmits collected
77 neural signals via Bluetooth to the external processor (Fig. 1c). As long as the external coil is
78 magnetically attached on the skin and paired with the internal coil, the implant will be powered
79 on. The implantable part of the NEO consists of a coin-size titanium alloy box, a coil, and epidural
80 electrodes. The entire system is sealed with medical silicone material (Fig. 1b). Two epidural
81 electrode strips are connected to the implant via electrode adaptors, with each electrode strip
82 featuring four contacts capable of both recording and stimulating. These eight electrode contacts
83 have a diameter of 3.2 mm and a center-to-center distance of 8 mm. The system operates at a
84 sampling rate of 1 kHz.

85 This design has two advantages in reducing invasiveness. First, it employs minimally invasive
86 epidural electrodes. These electrodes, placed on the dura mater, without penetrating the dura,
87 preventing a strong immune response and ensuring long-term stability. Second, the system utilizes
88 bidirectional wireless communication for both power and signal transmission (Fig. 1c). Wireless
89 communication reduces the risk of infection by eliminating the need for open wounds. The
90 implant does not contain a battery; instead, it is powered wirelessly via the coils, which also
91 handle bidirectional data transmission. This battery-free design ensures that the device's lifespan
92 is not limited by battery life. While a similar design has been widely adopted in cochlear
93 implants⁹, it has not yet been reported in the field of implanted brain-computer interfaces.

94 Signals are received by a relay station attached to the arm and transmitted to a computer
95 wirelessly. The computer decodes the patient's motor control intention continuously from the
96 neural data and drives the external pneumatic glove (Fig. 1a, Video 1). When the patient imagines
97 grasping and holding, the pneumatic glove grasps; when the patient wants to release the object, the
98 glove extends to release. In this unique configuration, the pneumatic glove not only acts as a BCI
99 actuator, but also provides sensory feedback to those neural fibers in the hand that may relay them
100 to the injured spinal cord sites. Thus, in every trial of BCI hand control, the intrinsic top-down
101 neural activities may have chance to meet with this bottom-up sensory feedback generated by the
102 successful grasping and releasing.

103 Study Participant

104 This study is part of a clinical trial for the implantable closed-loop BCI system (NEO)
105 (clinicaltrials.gov, NCT05920174), which was approved by the Xuanwu Hospital Ethics
106 Committee in April 2023. A patient was recruited in his 50s, who suffered a spinal cord injury in a
107 car accident more than 10 years, resulting in paralyzed both hand motor functions, making
108 grasping, holding, and pinching actions impossible (Video 2). However, limited right arm
109 functions are kept in this patient, which allows him to raise right forearm in a constrained angle.
110 Prior to NEO implantation, the patient underwent a neurological assessment and was diagnosed
111 with complete C4 spinal cord injury (AIS-A, Table S1, Fig. S1). Informed consent was obtained
112 from the participant.

113 Implantation of Minimally Invasive BCI

114 To obtain the most informative neural signals related to hand grasping with a minimal number of
115 electrodes, we performed preoperative planning for the epidural electrode implantation using
116 functional MRI (fMRI). Research indicates that the transmission of ascending signals is crucial for
117 SCI rehabilitation¹⁰. Therefore, our paradigm included fMRI imaging of both active and passive
118 grasping attempts. The active grasping paradigm requires the subject to perform motor imagery
119 based on visual cues, whereas the passive grasping paradigm requires the subject to perceive the
120 sensation of the experimenter assisting him in grasping and releasing. The active grasping
121 paradigm localized the sensory-motor area responsible for the patient's hand, while the passive
122 grasping paradigm assessed the residue ascending sensory signals (Fig. S2). Additionally, we
123 collected CT and structural MRI images of the patient to determine the precise implantation site.

124 The significant activation regions were projected from the fMRI onto a 3D model of the cortex,
125 using 3D modeling software to simulate electrode placement (Fig. S2). The position of the implant
126 was determined using skull structure obtained from CT images, selecting an area with suitable
127 thickness that can bury the titanium processor. The final plan was then output to a surgical
128 navigation system to guide the implantation procedure.

129 The minimally invasive BCI implantation surgery was completed in October 2023. Conducted
130 under general anesthesia, a coronal incision was made on the left scalp to place the internal
131 processor, coil, and electrode strips. Following the preoperative plan, a circular window was
132 created in the skull, exposing the dura mater, and the electrodes were sutured onto the dura mater
133 according to the planned coordinates. The bone flap was then repositioned and secured. A 3-4 mm
134 deep groove was created on the skull surface to embed the titanium implant, which was fixed
135 using bone screws, and the incision was closed. The patient was discharged within 24 hours after
136 all clinical observations were completed.

137 Postoperatively, we extracted the electrode positions from the postoperative CT images and
138 registered them to the preoperative MRI images, obtaining a map of the eight electrode positions.
139 The first four electrodes were placed above the precentral gyrus, while the latter four were above
140 the postcentral gyrus. Electrodes 2-3 (Brodmann area 6d) in the precentral gyrus and electrodes 7-
141 8 (Brodmann area 1) in the postcentral gyrus covered the most prominently activated hand areas
142 identified by fMRI during hand movement imagination (Fig. 1d, Fig. S2).

143 Decoding Brain-controlled Grasping Events

144 Based on the analysis on recorded epidural electrocorticography (eECoG) data (see Results: Long-
145 term Characteristics of Epidural Signals), we confirmed the wideband characteristics of eECoG,
146 which provides spatial resolution between subdural ECoG (sECoG) and scalp EEG. To accurately
147 decode the patient's natural grasping movement intention, our BCI decoder integrated frequency-
148 space-time domain information, by adopting multi-band frequency signal, restoring source space
149 activity, and maintaining invariance to signal amplitude over long periods.

150 Firstly, eECoG features were extracted by combining both spatial and spectral information into a
151 covariance matrix. To address long-term distribution shift in neural features¹¹, scale-invariant
152 Riemannian metrics was utilized for classification (see Appendix: Spatio-Spectral Riemannian
153 Geometry Decoding Method). Secondly, a hidden Markov model (HMM) was employed to
154 manage the temporal dependencies of continuous grasping actions, ensuring prediction accuracy
155 and stability (Fig. S3 and S4). This approach was compared with two commonly used BCI
156 decoding methods: a linear method, which uses linear spatio-temporal-spectral features¹, and the
157 Common Spatial Pattern (CSP) method¹², which uses multi-band spatial patterns (see Appendix:
158 The Control Decoding Methods).

159 Assessment of functional and neurological recovery

160 The regeneration of spinal connections induced by neuroplasticity from both internal and external
161 electrical activity has been explored and demonstrated^{3,13,14}. In this study, descending neural

162 activity was generated by voluntary movement intention from the sensorimotor cortex, while
163 ascending signals from muscle sensory feedback associated with pneumatic hand grasping.
164 Compared with epidural electrical stimulation over spinal cord to activate downstream muscles³,
165 our BCI driven process is more likely to trigger bi-directional neuronal coupling at injury sites. To
166 validate this hypothesis, we introduced electrophysiological measurements and neurological scales
167 to evaluate the effectiveness of the rehabilitation.

168 Somatosensory evoked potentials (SEPs) are used to assess sensory information conduction. SEPs
169 are elicited by electrically stimulating peripheral nerves, and the resulting neural activity travels
170 through the sensory pathways to the corresponding areas of the brain, such as the precentral and
171 postcentral gyri. Thus, SEPs reflect the transmission of sensory information from peripheral
172 muscles through the spinal cord to the brain, making them a useful tool for evaluating the extent
173 of spinal cord injury and the progress of recovery^{15,16}. SEP testing involves stimulating the
174 median, radial, and ulnar nerves of the patient's right arm (corresponding to C6-T1, C5-C8, and
175 C8-T1, respectively) with a constant current and recording the SEPs from the precentral and
176 postcentral gyri using the NEO epidural electrodes (Fig. 4a).

177 In this study, we employed two key assessments to quantify the neurological and functional
178 recovery of the subject. The international standards for neurological classification of spinal cord
179 injury (ISNCSCI) scale¹⁷ was used to evaluate the overall neurological status, including motor and
180 sensory capabilities, which is vital for determining the extent of spinal cord damage and subsequent
181 recovery. Additionally, the action research arm test (ARAT) scale¹⁸ was utilized to assess the finer
182 aspects of hand function, focusing on the subject's ability to handle objects, which is crucial for
183 evaluating the recovery of subtle motor skills of the upper limbs. These scales provided a
184 quantifiable measure for monitoring the improvements in neurological function and hand dexterity
185 over the course of the study.

186 Results

187 Long-term Characteristics of Epidural Brain Signals

188 Usually, brain electrophysiological recordings can be divided into three distinct levels: scalp
189 electroencephalography (EEG), subdural electrocorticography (sECoG), and intracortical single-
190 unit recordings. These methods vary in invasiveness and signal quality, with EEG being the safest
191 but having the lowest signal quality, and action potential recordings being the most invasive but
192 offering the highest signal quality. We propose that epidural ECoG (eECoG) represents a fourth
193 type, which provides higher safety than intracortical recordings⁷ and is considered minimally
194 invasive. However, long-term eECoG recordings have been scarce. With NEO BCI system, we
195 obtained substantial amount of eECoG signals for the first time. By analyzing these signals'
196 characteristics in spatial, temporal and spectral domains, we can maximize the use of eECoG
197 signal in the design of NEO BCI decoding methods.

198 The average event-related spectrum perturbation (ERSP) pattern of 1700 trials of eECoG during
199 imagined hand grasping versus rest is shown in Fig. 1e. The spectrum pattern exhibits a similar

200 dual-frequency feature with the subdural ECoG, including low-frequency (15-50 Hz) event-related
201 desynchronization (ERD) and high-frequency (>50 Hz) event-related synchronization (ERS)^{19,20}.

202 We compared the spatio-temporal-spectral characteristics of the patient's epidural ECoG with
203 subdural ECoG datasets²¹, the patient's own scalp EEG, and a published EEG dataset²². Scalp
204 EEG showed no significant ERSP above the low gamma (>40 Hz) frequency band ($p=0.42$,
205 independent t-test, Fig. 2a). Both epidural and subdural ECoG exhibited low-frequency ERD and
206 high-frequency ERS. It is particularly noteworthy that the frequency upper limit of eECoG can
207 exceed 200 Hz, which is significantly higher than that of scalp EEG (Fig. 2a). The power spectral
208 density of eECoG was lower than that of sECoG in most of frequency bands but obviously higher
209 than that of scalp EEG in the high-frequency range (20-75 Hz) (Fig. 2b). In spatial domain, by
210 comparing the relationship between channel correlation and electrode distance, we qualitatively
211 verified the spatial resolution differences among these three types of recordings. The correlation
212 between EEG channels decreased slowly with increasing electrode distance, indicating lowest
213 spatial resolution. The correlation between sECoG channels decreased most rapidly with
214 increasing electrode distance, indicating the highest spatial resolution, with eECoG showing
215 moderate spatial resolution (Fig. 2c).

216 In contrast to the signal degradation commonly observed in intracortical BCI^{6,23} in the current
217 epidural BCI setting, the quality of long-term eECoG signals improved along with training. All
218 electrodes' high gamma (HG) responses (55-95Hz) significantly increased over the period of 9
219 months ($p<0.001$, independent t-test, Fig. 2d), including the electrode No. 8 (Brodmann area 4)
220 which showed the strongest HG response during imagined hand movement. The low-frequency
221 power suppression and high-frequency power activation of electrodes in both the precentral and
222 postcentral gyrus during imagined hand movement were also continuously enhanced with training
223 (Fig. 2e-f). Additionally, the HG energy during resting states significantly increased with time
224 ($p<0.001$, independent t-test, Fig. 2h). We continuously measured the epidural electrode
225 impedance to monitor alterations in the patient's intracranial environment post-surgery, which
226 showed a slight increase in electrode impedance ($<600 \Omega$) at the beginning, and then a stabilized
227 impedance after 15 weeks (Fig. 2g).

228 BCI-assisted Natural Grasping

229 Based on the characteristics of eECoG, beta band (15-30Hz) and low gamma band (35-50Hz)
230 filtered signal, and high gamma (55-95Hz) power envelope were extracted to train a Riemannian-
231 based classifier. The BCI calibration was made within 10 minutes using a block design paradigm
232 alternating between imagined grasping and resting. For the BCI testing and rehabilitation training
233 task, the patient was instructed to use motor imagery to control a wearing pneumatic glove to
234 move an object from the center of a 3x3 grid to one of the eight surrounding cells (Fig. 3a, Fig.
235 S5). After 10 minutes of calibration, the patient achieved a decoding accuracy of 94% (Chance
236 level: 77%) and a grasp event detection F1 score (see Appendix: Model Training and Evaluation)
237 of 0.8 (Chance level: 0.09). The continuous increase in the patient's high-frequency amplitude of
238 eECoG usually affects the classification accuracy of linear decoders, but has minimal impact on
239 our Riemannian-based classifier¹¹. Over nine months, the patient's grasp event F1 score steadily
240 increased, surpassing 0.9 after three months (Fig 3i) and reaching an average of 0.91. The long-

241 term stability of the Riemannian method was superior to both Linear and CSP methods, with the
242 F1 score consistently improving (Fig. 3i) and feature distribution shifts being less pronounced
243 (Fig. S6). After 6 months of training, the subject's capability of grasping with the help of the BCI
244 system was evaluated. In the 3x3 grid test, the success rate was 100% within 10 seconds with BCI
245 grasping, compared to 35% without it (Fig. 3b-d, 181-185 days after implantation, Video 3). The
246 model's consistent and accurate predictions during the voluntary grasping demonstrate the
247 effectiveness of the BCI system. With BCI assistance, the dwelling time during grasping was
248 distributed between the start and end points, while without assistance, it was mostly around the
249 start point, indicating faster and smoother grasping with BCI (Fig. 3e-f, h). We compared the
250 performance of our system using EEG collected from the subject. The grasp event F1 score for the
251 EEG-based decoder was only 0.16 ± 0.11 (s.d.) (Chance level: 0.07), while for the eECoG, it was
252 0.90 ± 0.06 (s.d.) (Chance level: 0.09) (Fig. 3g). Notably, the average decoding delay with respect
253 to the screen cue was 1.23 ± 0.33 s, which is much lower than the EEG based motor imagery BCIs
254 (usually in the range of 2-5 s)²⁴⁻²⁶.

255 In a home use setting, the NEO BCI can assist with various tasks requiring grasping. However,
256 activities like eating and drinking usually elicit significant electromyographic (EMG) noise, which
257 interferes with the BCI decoder. Since the spatial distribution of EMG noise differs from that of
258 grasping movements, the Riemannian geometry method, which is highly sensitive to spatial
259 patterns, can filter out noise without supervised training (Fig. S7). Compared to the Riemannian
260 geometry method, the Linear and CSP methods had a false activation rate (FAR) of 100% during
261 chewing, while the Riemannian geometry method had a FAR of only 20% (Fig. 3j). Using the
262 Riemannian geometry BCI decoder, the patient could perform grasp-related daily tasks such as
263 eating and drinking (Video 4, 267 days after implantation), which was impossible before the BCI
264 implantation.

265 Hand Function Rehabilitation and Electrophysiology Assessment

266 We hypothesis that top-down neural electrical activity from the central and bottom-up sensory
267 feedback from the peripheral during BCI grasping can direct the neuronal projections at the spinal
268 cord injury sites that may facilitate neural rehabilitation^{8,27}. Indeed, during 9 months of continuous
269 training, significant neurophysiological and functional recovery was observed in the patient.
270 Changes in SEP signals from the radial, median, and ulnar nerves correspond to the recovery of
271 the sensory pathways at different levels of the spinal cord. The strongest and most stable SEP
272 responses were observed in electrode No.5 at Brodmann area 4 (Fig. 4b, Fig. S8). The radial nerve
273 (RN) corresponds to spinal segments (C5-T1, mostly C5) above the zone of partial preservation
274 (C5-C7), the median nerve (MN, C5-T1, mostly C6) is near the zone of partial preservation, and
275 the ulnar nerve (UN, C7-T1) is below it²⁸. Consequently, it is expected that SEPs from the radial
276 nerve will not show significant change, while SEPs from the median nerve will show some
277 improvement, and SEPs from the ulnar nerve might show less improvement. Indeed, over 9
278 months, the peak amplitude of SEPs elicited by median nerve stimulation in channel No. 5
279 increased by $12.2 \mu\text{V}$, whereas the radial nerve only get a $1.6 \mu\text{V}$ increase (Fig. 4c). Comparing
280 the first and ninth months, the mean amplitude of early (15-35ms) and late (40-80ms)
281 components (see Appendix: SEP Measurement) of median nerve SEPs increased significantly
282 across most channels, with channel No.5 showing the biggest increase of $5.0 \mu\text{V}$ in the early

283 component. The late component of ulnar nerve SEPs increased significantly in most channels,
284 with channel No.4 showing the biggest increase of 2.1 μ V, but the early component did not show
285 a significant increase. The radial nerve showed no significant increase for either component in all
286 channels but channel No.4, which showed a significant increase for late component (Fig. 4d, Fig.
287 S9, bootstrap permutation test, FDR corrected, statistical p-values in Table S2).

288 The patient's neurological scales and hand function assessment corresponded well with the SEP
289 changes. The patient's upper limb motor score on the ISNCSCI scale increased by 5 points over
290 nine months, with changes concentrated in the C5-C8 segments, and the motor level dropping
291 from C5 to C6. The sensory score increased by 8 points, peaking at 11 points in the fifth month,
292 mostly in the C5-T4 segments (Fig. 5a-b, Table S1). The ARAT scale, which evaluates dexterous
293 hand functions, including grasp, grip, pinch and gross movements, showed a 16-point
294 improvement in the patient's right hand (contralateral to the BCI electrodes) nine months post-
295 surgery. Surprisingly, a 11-point improvement was also observed in the left hand (ipsilateral to the
296 BCI electrodes). The main improvement was in the grasp score, with the trained right hand
297 showing more improvement than the left hand (Fig. 5d, Table S3). For example, in the ARAT
298 grasp test, the patient was able to grasp a 5 cm wooden block faster in the fifth month compared to
299 the third month (3.9 s vs. 6.1 s) and was also able to successfully grasp a 7.5 cm wooden block in
300 the fifth month (Fig. 5c, e-f), which is impossible before that. The patient completed the ARAT
301 grasping part test before the surgery. Compared to the preoperative results, the grasping speed and
302 success rate for 5 cm wooden block and 7.5 cm wooden sphere were significantly improved nine
303 months after the surgery for the contralateral hand (Video 2). It is noteworthy that, due to the
304 patient's use of Baclofen and Pregabalin in the sixth month, there was a sudden decrease in
305 sensory and motor scores, and an immediate recovery of both scores following the stop of drug
306 use since the seventh month (Fig. 5a and 5b).

307 Discussion

308 This study presents the first human trial of a wireless minimally invasive epidural BCI system,
309 with which a novel brain-spine rehabilitation pathway was established entirely based on the
310 patient's intrinsic neural activities. This pathway enabled a patient with a complete C4 spinal cord
311 injury to regain voluntary hand grasping function. Furthermore, active rehabilitation training with
312 the BCI led to a prominent recovery of hand functions. Significant and consistent improvements
313 were observed in neurological scales, hand function assessments, and electrophysiological tests.

314 Implantable brain-computer interfaces often face a trade-off between performance and safety.
315 Typically, a higher channel number and more aggressive contact design leads to higher
316 performance but lower stability^{6,29}. The wireless minimally invasive epidural BCI system
317 developed in this study, featuring wireless powering and signal transmission with a battery-free,
318 closed-wound design, ensures long-term safety and stability for home use while effectively
319 facilitating hand function restoration and rehabilitation. Although BCIs based on microelectrode
320 implants can achieve similar functions, their long-term stability is limited by issues such as
321 electrode displacement and glial cell encapsulation, necessitating frequent recalibration^{6,30}. Some
322 BCIs using subdural cortical electrodes have been reported to maintain high long-term stability,

323 requiring no recalibration for 2-6 months^{29,31}. However, subdural electrodes pose a higher risk of
324 adverse effects such as hematomas, intracranial hemorrhage, brain infarction, and cerebral edema
325 due to direct pressure on brain tissue^{7,32}. In contrast, minimally invasive epidural brain-computer
326 interfaces offer significant advantages in long-term stability. The electrodes are placed outside the
327 dura mater, providing structural support without damaging or compressing brain tissues.
328 Consequently, the minimally invasive epidural electrodes exhibit better long-term stability, with
329 signal quality improving over a nine-month period (Fig. 2h). Additionally, decoding performance
330 remains stable over nine months with only 10 minutes of calibration (Fig. 3i).

331 In this study, we demonstrated for the first time that a minimally invasive BCI system, relying
332 solely on the patient's intrinsic sensory ascending and motor descending signals, can likely direct
333 the spinal circuit reconstruction, thus, to facilitate the rehabilitation of upper limb functions in a
334 patient with complete spinal cord injury. Previous studies have validated the effectiveness of
335 brain-controlled spinal cord injury rehabilitation systems based on similar principle^{3,33,34}, but they
336 largely depend on electrical stimulation of limbs³⁴ or the spinal cord³ to induce recovery. Our
337 research confirmed the feasibility of directly using the intrinsic ascending and descending neural
338 activities to facilitate upper limb rehabilitation. Additionally, there is a hypothesis that electrical
339 epidural stimulation of the spinal cord enhances the excitability of spinal nerves, thereby inducing
340 neural circuit remodeling^{8,14}. This method complements our approach and could be combined in
341 the future to improve brain-controlled upper limb rehabilitation outcomes.

342 Our study also established a quantitative assessment method for neurological function
343 rehabilitation based on SEP (somatosensory evoked potential) using NEO BCI system. The trend
344 of changes in the amplitude of different SEP components was highly consistent with the patient's
345 rehabilitation progress. At the sixth month, the patient was taking Baclofen and Pregabalin, both
346 of which have inhibitory effects on the central nervous system. These medications exert global
347 suppression on the central system, while SEP, as a primary cortical response to sensory
348 information, is theoretically less affected by such medications compared to higher-level brain
349 activities involved in subjective sensory perception. The results showed that SEP test outcomes
350 were less disturbed than the sensory scores on the ISNCSCI scale, more accurately reflecting the
351 connectivity of spinal neural circuits (Fig. 5a and 5b). Given that similar medications are
352 commonly used by SCI patients, the stability of SEP provides a better assessment of the patient's
353 sensory perception.

354 This study is a prospective investigation of a novel brain-computer interface, reporting results
355 from a single subject. Consequently, the rehabilitation effects for patients with different injury
356 locations or severities remain uncertain. However, our approach holds potential for application to
357 other spinal cord injury patients. Firstly, the case we reported is an AIS-A level case, representing
358 the most severe level of spinal cord injury. Patients with less severe injuries would have more
359 residual spinal connections, providing higher chance for rehabilitation. Secondly, with nine
360 months of home use, our system is proven to be highly reliable and scalable, with high decoding
361 accuracy and long-term stability. Similar patients can quickly calibrate and use the system at home
362 for long-term, effective rehabilitation training.

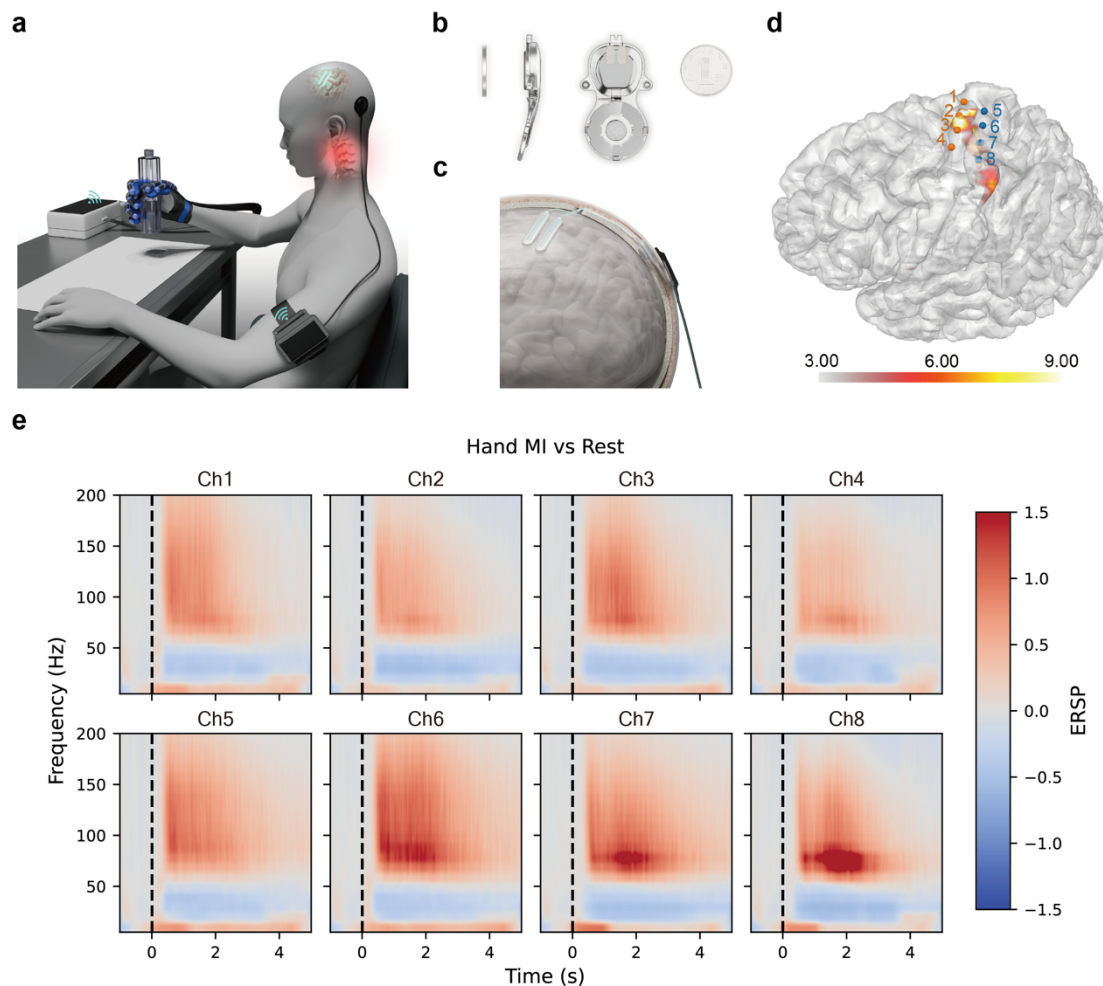
363 Acknowledgement

364 We thank our volunteer patient and his family for their commitment and trust. We thank Sichang
365 Chen and Lin Liu from Xuanwu Hospital of Capital Medical University, Yujing Wang and Xiaoshan
366 Huang from Neuracle Technology Co., Zheng Yan from Huaqiao University, Ze'ao Xiong, Ruwei
367 Yao, Yunjing Li, Yujing Lin, Le Yu, Yichao Li from Tsinghua University, and Zhouxingyu Yan from
368 John Hopkins University for their help in this work.
369

370 Reference

- 371 1. Benabid, A. L. *et al.* An exoskeleton controlled by an epidural wireless brain–machine interface
372 in a tetraplegic patient: a proof-of-concept demonstration. *Lancet Neurol.* **18**, 1112–1122 (2019).
- 373 2. Moses, D. A. *et al.* Neuroprosthesis for Decoding Speech in a Paralyzed Person with Anarthria.
374 *N. Engl. J. Med.* **385**, 217–227 (2021).
- 375 3. Lorach, H. *et al.* Walking naturally after spinal cord injury using a brain–spine interface. *Nature*
376 **618**, 126–133 (2023).
- 377 4. Samejima, S. *et al.* Brain-computer-spinal interface restores upper limb function after spinal cord
378 injury. *IEEE Trans. Neural Syst. Rehabil. Eng.* **29**, 1233–1242 (2021).
- 379 5. Willett, F. R., Avansino, D. T., Hochberg, L. R., Henderson, J. M. & Shenoy, K. V. High-
380 performance brain-to-text communication via handwriting. *Nature* **593**, 249–254 (2021).
- 381 6. Patel, P. R. *et al.* Utah array characterization and histological analysis of a multi-year implant in
382 non-human primate motor and sensory cortices. *J. Neural Eng.* **20**, (2023).
- 383 7. Branco, M. P., Geukes, S. H., Aarnoutse, E. J., Ramsey, N. F. & Vansteensel, M. J. Nine decades
384 of electrocorticography: A comparison between epidural and subdural recordings. *Eur. J.*
385 *Neurosci.* **57**, 1260–1288 (2023).
- 386 8. Anderson, M. A. *et al.* Natural and targeted circuit reorganization after spinal cord injury. *Nat.*
387 *Neurosci.* **25**, 1584–1596 (2022).
- 388 9. Zeng, F.-G., Rebscher, S., Harrison, W., Sun, X. & Feng, H. Cochlear Implants: System Design,
389 Integration, and Evaluation. *IEEE Rev. Biomed. Eng.* **1**, 115–142 (2008).
- 390 10. Formento, E. *et al.* Electrical spinal cord stimulation must preserve proprioception to enable
391 locomotion in humans with spinal cord injury. *Nat. Neurosci.* **21**, 1728–1741 (2018).
- 392 11. Congedo, M., Barachant, A. & Bhatia, R. Riemannian geometry for EEG-based brain-computer
393 interfaces; a primer and a review. *Brain-Computer Interfaces* **4**, 155–174 (2017).
- 394 12. Koles, Z. J. The quantitative extraction and topographic mapping of the abnormal components
395 in the clinical EEG. *Electroencephalogr. Clin. Neurophysiol.* **79**, 440–447 (1991).
- 396 13. Inanici, F., Brighton, L. N., Samejima, S., Hofstetter, C. P. & Moritz, C. T. Transcutaneous
397 Spinal Cord Stimulation Restores Hand and Arm Function after Spinal Cord Injury. *IEEE Trans.*
398 *Neural Syst. Rehabil. Eng.* **29**, 310–319 (2021).
- 399 14. Moritz, C. *et al.* Non-invasive spinal cord electrical stimulation for arm and hand function in
400 chronic tetraplegia : a safety and efficacy trial. *Nat. Med.* **30**, 18–24 (2024).
- 401 15. Kramer, J. K., Taylor, P., Steeves, J. D. & Curt, A. Dermatomal somatosensory evoked potentials
402 and electrical perception thresholds during recovery from cervical spinal cord injury.
403 *Neurorehabil. Neural Repair* **24**, 309–317 (2010).
- 404 16. Kramer, J. L. K., Moss, A. J., Taylor, P. & Curt, A. Assessment of posterior spinal cord function
405 with electrical perception threshold in spinal cord injury. *J. Neurotrauma* **25**, 1019–1026 (2008).
- 406 17. Rupp, R. *et al.* International standards for neurological classification of spinal cord injury. *Top.*
407 *Spinal Cord Inj. Rehabil.* **27**, 1–22 (2021).
- 408 18. Yozbatiran, N., Der-Yeghiaian, L. & Cramer, S. C. A standardized approach to performing the
409 action research arm test. *Neurorehabil. Neural Repair* **22**, 78–90 (2008).
- 410 19. Miller, K. J. *et al.* Spectral changes in cortical surface potentials during motor movement. *J.*
411 *Neurosci.* **27**, 2424–2432 (2007).
- 412 20. Bundy, D. T. *et al.* Characterization of the effects of the human dura on macro- and micro-

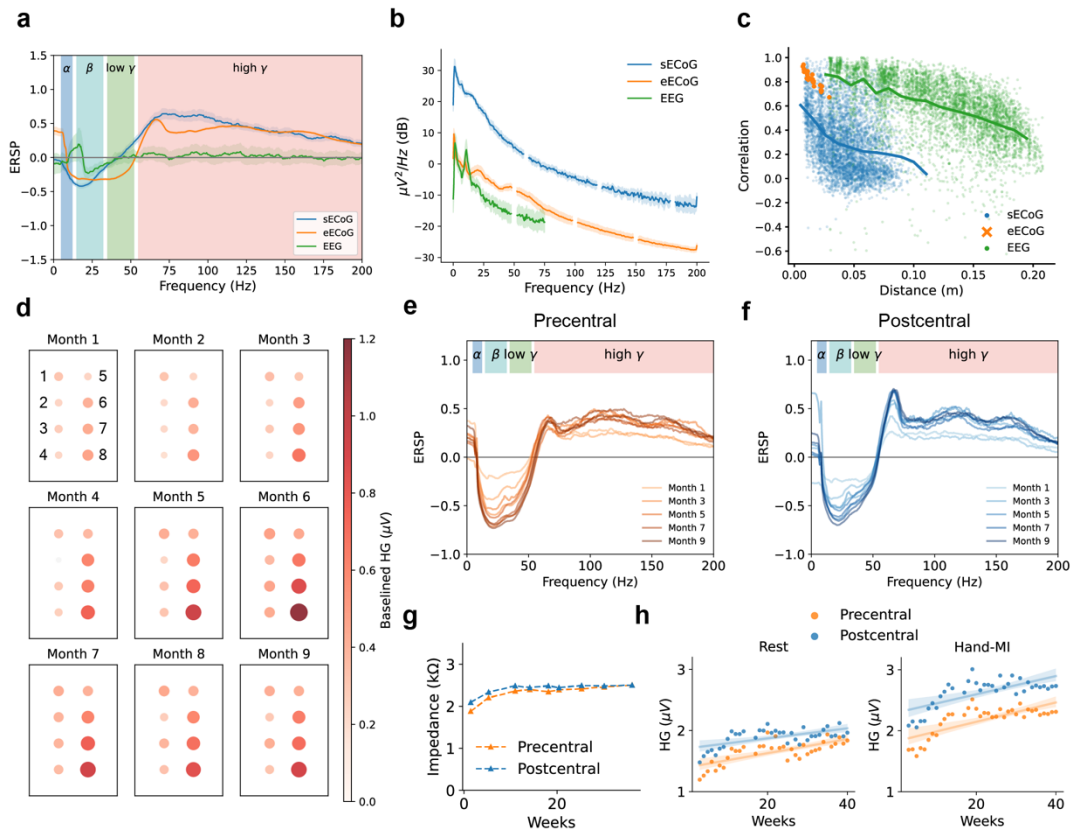
- 413 electrocorticographic recordings. *J. Neural Eng.* **11**, (2014).
- 414 21. Miller, K. J. A library of human electrocorticographic data and analyses. *Nat. Hum. Behav.* **3**,
415 1225–1235 (2019).
- 416 22. Schalk, G., McFarland, D. J., Hinterberger, T., Birbaumer, N. & Wolpaw, J. R. BCI2000: A
417 General-Purpose Brain-Computer Interface (BCI) System. *IEEE Trans. Biomed. Eng.* **51**, 1034–
418 1043 (2004).
- 419 23. Black, B. J. *et al.* Chronic recording and electrochemical performance of utah microelectrode
420 arrays implanted in rat motor cortex. *J. Neurophysiol.* **120**, 2083–2090 (2018).
- 421 24. Pfurtscheller, G., Linortner, P., Winkler, R., Korisek, G. & Müller-Putz, G. Discrimination of
422 motor imagery-induced EEG patterns in patients with complete spinal cord injury. *Comput. Intell.*
423 *Neurosci.* **2009**, 1–6 (2009).
- 424 25. Firat Ince, N., Arica, S. & Tewfik, A. Classification of single trial motor imagery EEG recordings
425 with subject adapted non-dyadic arbitrary time-frequency tilings. *J. Neural Eng.* **3**, 235–244
426 (2006).
- 427 26. Lawhern, V. J. *et al.* EEGNet: A compact convolutional neural network for EEG-based brain-
428 computer interfaces. *J. Neural Eng.* **15**, (2018).
- 429 27. Asboth, L. *et al.* Cortico–reticulo–spinal circuit reorganization enables functional recovery after
430 severe spinal cord contusion. *Nat. Neurosci.* **21**, 576–588 (2018).
- 431 28. Grisolia, J. S. & Wiederholt, W. C. Short latency somatosensory evoked potentials from radial,
432 median and ulnar nerve stimulation in man. *Electroencephalogr. Clin. Neurophysiol.* **50**, 375–
433 381 (1980).
- 434 29. Milekovic, T. *et al.* Stable long-term BCI-enabled communication in ALS and locked-in
435 syndrome using LFP signals. *J. Neurophysiol.* **120**, 343–360 (2018).
- 436 30. Barrese, J. C. *et al.* Failure mode analysis of silicon-based intracortical microelectrode arrays in
437 non-human primates. *J. Neural Eng.* **10**, (2013).
- 438 31. Luo, S. *et al.* Stable Decoding from a Speech BCI Enables Control for an Individual with ALS
439 without Recalibration for 3 Months. *Adv. Sci.* **10**, 1–12 (2023).
- 440 32. Fountas, K. N. & Smith, J. R. Subdural electrode-associated complications: A 20-year experience.
441 *Stereotact. Funct. Neurosurg.* **85**, 264–272 (2007).
- 442 33. Donati, A. R. C. *et al.* Long-Term Training with a Brain-Machine Interface-Based Gait Protocol
443 Induces Partial Neurological Recovery in Paraplegic Patients. *Sci. Rep.* **6**, 1–16 (2016).
- 444 34. Jovanovic, L. I. *et al.* Restoration of Upper Limb Function after Chronic Severe Hemiplegia: A
445 Case Report on the Feasibility of a Brain-Computer Interface-Triggered Functional Electrical
446 Stimulation Therapy. *Am. J. Phys. Med. Rehabil.* **99**, e35–e40 (2020).
- 447
- 448



449

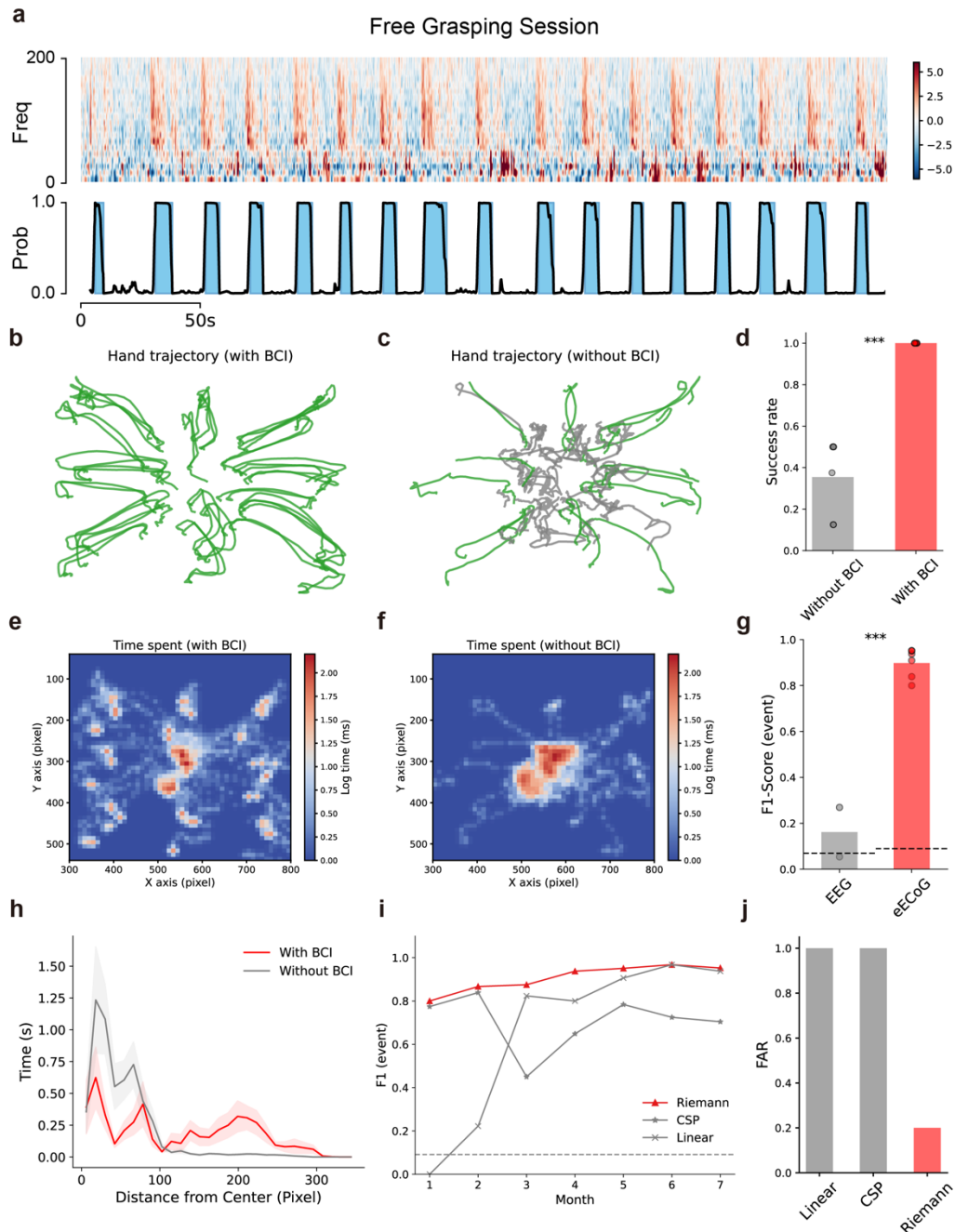
450 **Figure 1 NEO system design and epidural signal characteristics.** a, Diagram of the NEO brain-
451 computer interface (BCI) system. The NEO BCI system transmits epidural ECoG signal through a coil
452 to an external device attached on the patient's arm. The external device sends the signals to the host
453 computer, where an algorithm decodes the patient's grasping intention and drives a wearable pneumatic
454 glove to grasp objects. When the patient stops imagining the grasp, the pneumatic glove is driven to open
455 and release the object. b, Structure of the NEO implant. The upper part is the implant, and the lower part
456 is the internal coil. c, The NEO implant. Electrodes are fixed on the surface of the dura mater and
457 connected to the implant through a skull tunnel. The external coil is magnetically attached through the
458 skin, transmitting signals and power. d, Epidural electrode positions. The orange and blue dots represent
459 the electrodes on the precentral and postcentral gyrus, respectively. The heat map overlaying the cortical
460 surface represents functional MRI activation significance values (negative logarithm of p values). e,
461 Event-related spectral perturbation (ERSP) during imagined grasping. The spectral pattern exhibits a
462 typical dual-frequency characteristic, including low-frequency (15-50 Hz) suppression and high-
463 frequency (>50 Hz) activation. Hand-MI: Hand Motor Imagery.

464



465

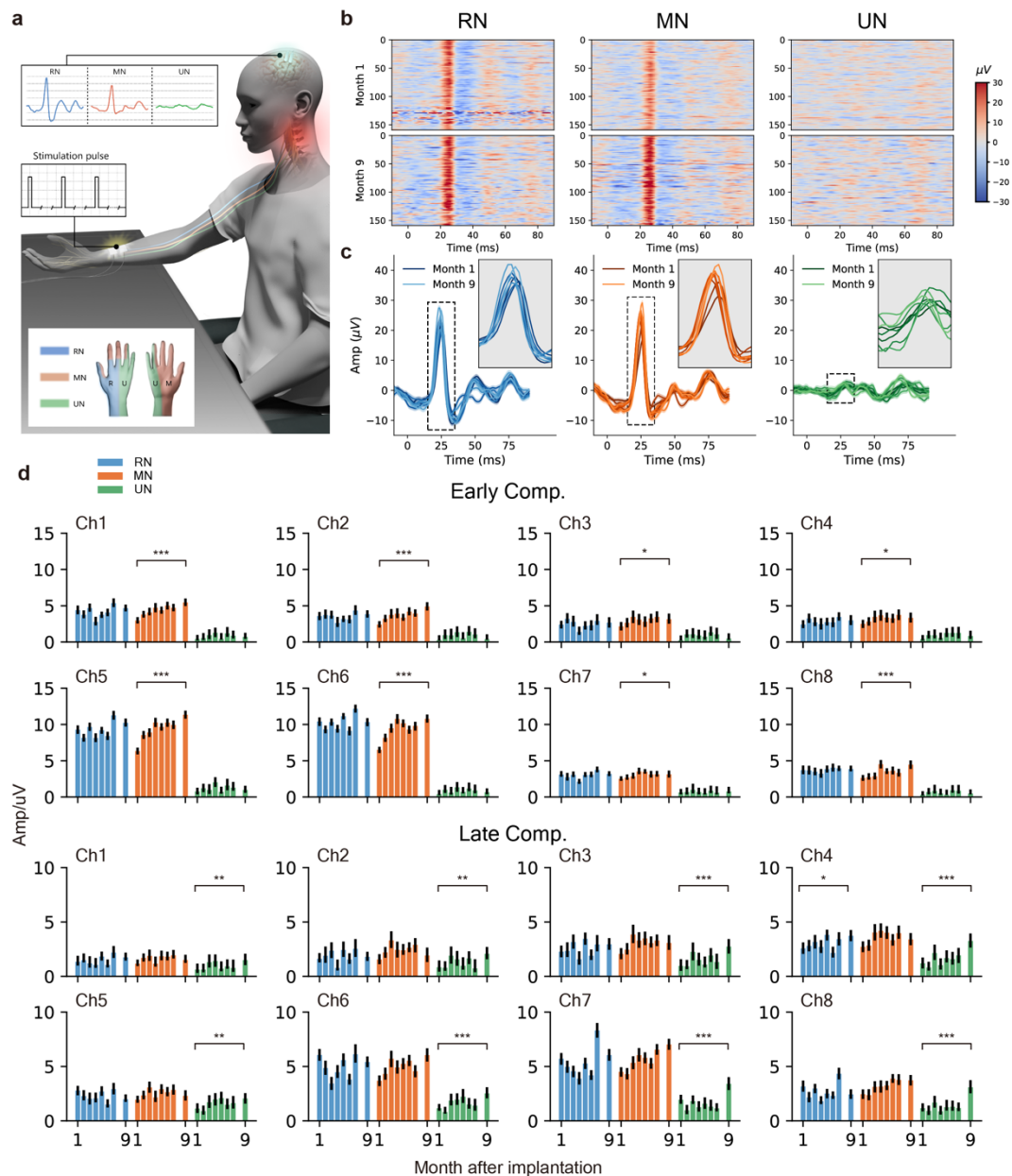
466 **Figure 2 Long-term spatio-temporal-spectral characteristics of epidural signals.** a, Comparison of
 467 event-related spectral perturbations (ERSP) among subdural ECoG, epidural ECoG, and scalp EEG.
 468 Epidural ECoG exhibits an effective frequency band range similar to subdural ECoG. b, Comparison of
 469 Power spectral density (PSD) among the three types of electrophysiological recordings. Subdural ECoG
 470 has the highest amplitude, and epidural ECoG has a higher amplitude in the higher frequency band (30-
 471 70 Hz) compared to scalp EEG. The PSD excludes the power line frequencies. c, Relationship between
 472 channel signal correlation and electrode distance. d, Trend of high-frequency energy (55-95 Hz) spatial
 473 patterns of epidural ECoG during imagined hand movements. Long-term training significantly enhances
 474 high-frequency activity in the ECoGs of all channels during motor imagery (Month 1 vs. Month 6,
 475 $p < 0.001$, independent t-test). Channels where the HG response is not significantly greater than zero are
 476 marked as gray. e-f, Trend of the average ERSP of precentral and postcentral electrodes, with each curve
 477 representing the average ERSP of one month's hand motor imagery data. Both low-frequency ERD and
 478 high-frequency ERS gradually increase with training. g, Impedance changes of precentral and postcentral
 479 electrodes. h, Trend in high-frequency energy (55-95 Hz, un-baselined) of precentral and postcentral
 480 electrodes during rest and hand motor imagery, both showing significant positive correlations (resting:
 481 $r = 0.67$, $p < 0.001$; motor imagery: $r = 0.73$, $p < 0.001$). In a, b, and c, subdural ECoG data are from the Kai
 482 Miller dataset²¹; a and b use scalp EEG from the patient's own recordings; c uses scalp EEG from the
 483 BCI2000 dataset²². Hand-MI: Hand Motor Imagery. HG: High-Gamma band power.



484

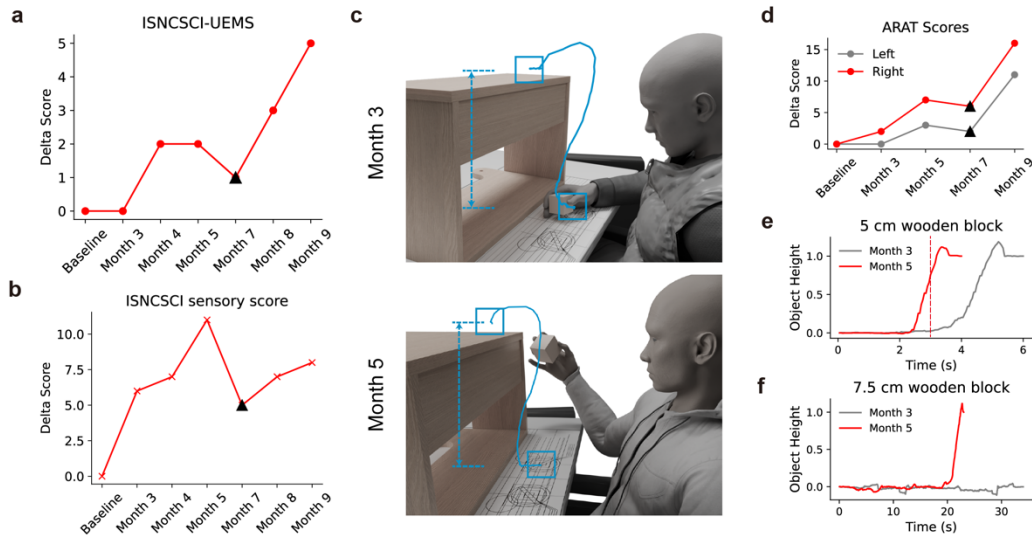
485 **Figure 3 Minimally invasive epidural BCI for motor assistance.** a, Example of BCI testing data and
 486 decoded confidences. Single-trial epidural ECoG induced by grasping intention has a high signal-to-
 487 noise ratio (upper panel). The blue shading indicates the time range of the grasping action as determined
 488 by the decoder (lower panel). b-c, Hand movement trajectories of the patient performing the object
 489 moving task with BCI assistance (b) or unaided (c), recorded by a top-down camera and identified by a
 490 keypoint detection model. The green lines represent the successful trials whereas the grey lines represent
 491 the failed trials. d, With BCI assistance, the patient's success rate of moving the object to the designated
 492 position within 10 seconds is 100%, whereas, without BCI assistance, the success rate is only 35%. e-f,
 493 Logarithmic spatial distribution of the dwelling time with BCI assistance (e) or unaided (f). With BCI
 494 assistance, the dwelling time is clustered in the target start and end points, while unaided, the time was
 495 mostly spent in the start area. g, F1 scores for detecting grasping events using epidural ECoG and scalp

496 EEG. The black dashed line represents the chance level. Epidural ECoG detection F1 scores are
497 significantly higher than those of scalp EEG. h, Distribution of the relationship between time spent and
498 distance to the central start point. With BCI assistance, the patient can pick up the object and move to
499 the edge more quickly. i, Changes in the F1 score of the decoding algorithm for detecting grasping events
500 over 7 months. The Riemannian geometry-based decoding method shows long-term stability,
501 outperforming the control linear method and Common spatial pattern (CSP) method. The gray dashed
502 line represents the chance level. j, Tolerance of different models to electromyographic (EMG) noise
503 caused by chewing during daily use. Due to its high specificity to spatial patterns, the Riemannian
504 geometry method shows the best robustness, compared to the linear method and the CSP method. FAR:
505 False Activation Rate.
506



507

508 **Figure 4 Electrophysiological rehabilitation assessments.** a, Diagram of sensory evoked potential (SEP)
 509 measurement. Functional stimulators were used to stimulate the patient's radial, median, and ulnar
 510 nerves transcutaneously, and SEP activities were recorded from NEO epidural electrodes. b, Trial
 511 images of SEP waveforms (Electrode No. 5) for the patient's radial nerve (left panel), median nerve
 512 (center panel), and ulnar nerve (right panel) at the 1st and 9th months. c, SEP waveforms over 9
 513 months, with colors from dark to light representing SEP waveforms over the 9 months (Electrode
 514 No. 5). d, Relationship of average amplitude changes over time for early SEP components (15-35 ms,
 515 top) and late SEP components (40-80 ms, bottom) for each nerve, channel, and month. *: $p < 0.05$, **: $p < 0.01$, ***: $p < 0.001$, bootstrap permutation test, FDR corrected. MN: median nerve; RN: radial nerve;
 516 UN: ulnar nerve.
 517
 518



519

520 **Figure 5 Neurological and functional rehabilitation assessments.** a-b, Changes in key muscle strength of the
521 upper limbs and sensory scores in the ISNCSCI scale. Motor and sensory scores encountered a decrease
522 in the 7th month (black triangles) due to the patient's use of antispasmodic medication. c, The patient
523 grasping and releasing a 5 cm block in the Action Research Arm Test (ARAT) at the 3rd and 5th months.
524 The red curve represents the block trajectory, the boxes mark the start and end points, and the dashed
525 lines indicate the height of the lift. d, Changes in ARAT scores over the course of training. The 7th month
526 was marked as a black triangle. e-f, Curves for lift heights over time of 5 cm and 7.5 cm block grasp
527 tasks in ARAT at the 3rd and 5th months, with the red dashed line indicating the time point shown in e.
528 Trajectories were obtained from video recordings and manually annotated.

529

530

531 **Video 1 Mind to motion: NEO BCI overview**

532 This video outlines the basic setup of the NEO brain-computer interface (BCI) system. First, the
533 NEO implant is powered on. Next, the pneumatic glove is attached and configured. Once connected
534 to the controller, the NEO system transmits epidural ECoG signals in real-time. Finally, the subject
535 is able to control the pneumatic hand using his thoughts. Link to view online:

536 <https://cloud.tsinghua.edu.cn/f/436ac7de6df548d68088/>

537

538 **Video 2 ARAT hand function Test**

539 This video demonstrates the subject's improvement in hand function following a 9-month training
540 period. It compares the subject's performance on ARAT tasks before surgery (baseline) and at the
541 9-month mark for both hands. For the right hand, grasping tasks involving 5 cm, and 7.5 cm cubes,
542 as well as a 7.5 cm sphere, are compared between the baseline and 9th month. For the left hand, the
543 grasping task with a sharpening stone is evaluated. Link to view online:

544 <https://cloud.tsinghua.edu.cn/f/84948e6e6b0a4b4e9f2c/>

545

546 **Video 3 NEO BCI for grasping and object moving task.**

547 This video demonstrates how the NEO system assists in hand function. With the help of the NEO
548 BCI system, the subject successfully lifts a bottle of water and moves it to the designated target area.
549 Link to view online:

550 <https://cloud.tsinghua.edu.cn/f/199548a0cff549d4b45e/>

551

552 **Video 4 NEO for Independent Home Use.**

553 This video highlights how the NEO system enhances the subject's daily life. Using the NEO system,
554 the subject can independently eat with a customized fork and drink from either a plastic bottle or
555 glass. Link to view online:

556 <https://cloud.tsinghua.edu.cn/f/96f88f90731d45428607/>

557